View metadata, citation and similar papers at core.ac.uk
brought to you by CORE
provided by CiteSeerX

CMOS-compatible 75 mW erbium-doped distributed feedback laser

Ehsan Shah Hosseini,[1,*] Purnawirman,[1] Jonathan D. B. Bradley,[1] Jie Sun,[1] Gerald Leake,[2] Thomas N. Adam,[2] Douglas D. Coolbaugh,[2] and Michael R. Watts[1]

[1]*Photonic Microsystems Group, Research Laboratory of Electronics, Massachusetts Institute of Technology, 77 Massachusetts Avenue, Cambridge, Massachusetts 02139, USA*

[2]*College of Nanoscale Science and Engineering, University at Albany, State University of New York, 257 Fuller Road, Albany, New York 12203, USA*

**Corresponding author: ehsansh@mit.edu*

Received April 1, 2014; accepted April 7, 2014;
posted April 22, 2014 (Doc. ID 209327); published May 19, 2014

On-chip, high-power, erbium-doped distributed feedback lasers are demonstrated in a CMOS-compatible fabrication flow. The laser cavities consist of silicon nitride waveguide and grating features, defined by wafer-scale immersion lithography and an erbium-doped aluminum oxide layer deposited as the final step in the fabrication process. The large mode size lasers demonstrate single-mode continuous wave operation with a maximum output power of 75 mW without any thermal damage. The laser output power does not saturate at high pump intensities and is, therefore, capable of delivering even higher on-chip signals if a stronger pump is utilized. The amplitude noise of the laser is investigated and the laser is shown to be stable and free from self-pulsing when the pump power is sufficiently above threshold. © 2014 Optical Society of America

OCIS codes: (130.0130) Integrated optics; (130.2790) Guided waves; (130.3120) Integrated optics devices; (140.3460) Lasers; (140.3490) Lasers, distributed-feedback.
http://dx.doi.org/10.1364/OL.39.003106

Efficient, low noise, narrow band and stable on-chip lasers are essential for a variety of important applications, ranging from integrated analog photonics and microwave generation to coherent communications and light detection and ranging (LiDAR). Recently, two methods have shown the greatest promise for delivering high performance, integrated silicon-compatible lasers; namely, hybrid integration of silicon-on-oxide (SOI) waveguides with III-V semiconductor gain media [1–3], and erbium/ytterbium-doped glasses on silicon [4–6]. Despite the possibility of high efficiency electrically pumped lasing, III-V/SOI hybrid lasers tend to exhibit broad linewidths and correspondingly high phase noise levels due to their limited internal quality factors, large spontaneous emission rate, and large thermo-optic coefficients [7]. Furthermore, integration of III-V chips or wafers to silicon is a complicated fabrication process that can lead to low yield and high cost.

Wafer-bonded hybrid devices are subject to severe Joule heating because the thick, buried oxide layer of the SOI substrate is a large thermal barrier, preventing heat dissipation from the laser cavity and significantly degrading the performance of these quantum well-based devices. Consequently, high-power, single-mode operation of such devices is challenging unless complicated approaches, such as silicon-on-diamond substrates or thermal shunts, are employed. To our knowledge, the highest power reported from a hybrid distributed feedback (DFB) device was 14 mW, which was achieved with a cooled substrate and was extremely sensitive to environmental change [1]. Alternatively, the die-to-metal bonding approach, recently demonstrated by Creazzo *et al.*, despite alleviating the thermal conductance issue, was too involved to be wafer-scale, and the maximum 9 mW output still too susceptible to substrate temperature changes, with the output power dropping to below 5 mW at 80°C and the wavelength changing with ~0.1 nm/°C [3]. The other alternative approaches, namely Raman scattering [8] and germanium-on-silicon [9], suffer from high two-photon absorption at 1550 nm and extremely high threshold currents, respectively.

In this Letter, we demonstrate wafer-scale, high-power lasers created in a CMOS-compatible process, utilizing erbium's broadband gain (1530–1610 nm [10,11]) when co-sputtered into aluminum oxide; a low loss, high refractive index (n 1.65 at 1550 nm), and temperature-independent medium [11–13].

To avoid the necessity of incorporating Er into the standard CMOS process, an inverted ridge waveguide design is used, in which the high resolution patterns, including the waveguide ridge and gratings, are lithographically defined in a plasma-enhanced chemical vapor deposition (PECVD) frontend silicon nitride (SiN). The Al_2O_3:Er glass layer can then be deposited as a backend process step without any further etching or processing required. This approach enables large-scale production of erbium-doped waveguide lasers and integration with silicon nitride-passive components on silicon photonic chips. The structure of waveguides used in this study is shown in Fig. 1(a) and the intensity profile of the mode is depicted in Fig. 1(b).

Two important factors to consider in designing the waveguides are the overlap of the laser mode with the gain material (i.e., the electric field intensity confinement factor [14]) and also the signal–pump overlap (i.e., overlap factor [10,15]). For the structures used in this work (shown in Fig. 1), the width of the SiN core can be adjusted to control the field confinement, signal–pump overlap, and the mode size while the waveguide remains single-mode for waveguides as wide as 4 μm. To be capable of handling large pump powers without thermal damage, the mode size is maximized by choosing a 4 μm core. Figure 1(b) depicts the mode intensity distribution simulated with a finite difference mode solver for the

 © 2014 Optical Society of America

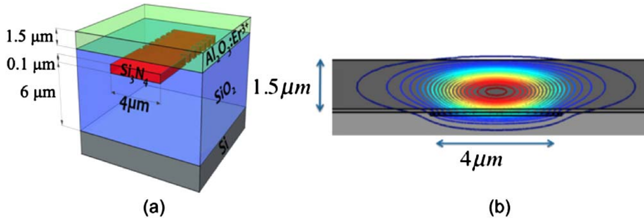

Fig. 1. Waveguides used in this work. (a) Layers used for constructing the waveguide structure within wafer-scale fabrication flow. High-definition masks are used to create waveguides and gratings in the SiN layer, and an erbium-doped glass is deposited as a blanket film. (b) Intensity profile of an inverted ridge waveguide mode with a 4 μm SiN core. The 1563 nm mode is mainly confined in the erbium-doped glass.

1563 nm wavelength. This novel design allows an excellent overlap between the guided mode and the Al_2O_3:Er, with a confinement factor of 83% and a pump–signal overlap of 90% calculated by solving for both the 1480 nm pump and 1563 nm laser.

Even though a small portion of the field intensity interacts with the SiN core and the oxide cladding/substrate, low-threshold lasing necessitates sufficiently low loss films. Few reports on PECVD silicon nitride waveguide applications have been published, owing to high losses caused by film roughness and infrared absorption [16]. While thermal oxide and low pressure plasma-enhanced chemical vapor deposition (LPCVD) silicon nitride allows low loss films [17,18] and low threshold lasers [19], the necessity of future integration with active silicon photonics devices and compatibility with a standard foundry flow entails PECVD-deposited core and cladding, to eliminate silicon consumption and minimize the thermal budget. A 6 μm-thick plasma-enhanced tetraethylorthosilicate (pTEOS) SiO_2 layer was grown, followed by deposition of a 0.1 μm-thick PECVD SiN layer. The gas ratios and plasma conditions were optimized for a low hydrogen content and SiN index of refraction of $n = 2$ at 1550 nm. Both layers were chemically mechanically polished (CMPed) to reduce losses due to surface roughness. The silicon nitride layer was subsequently annealed at 1050°C for 72 min to reduce absorption due to Si–H and N–H bonds around 1.52 μm [20]. The nitride layer was then patterned using 193 nm immersion lithography and reactive ion etching. The sidewall roughness was minimized by a short 900°C wet oxidation, followed by an HF dip. Subsequently, a PECVD SiO_2 layer was deposited and CMPed to a final height of 0.1 μm above the patterned silicon nitride core. Trenches for dicing and fiber end coupling were then etched into the edges of the dies by deep oxide and silicon etching. Finally, the wafers were transferred from the CMOS foundry, diced into individual dies, and an Al_2O_3:Er layer was deposited by reactive co-sputtering, using a process similar to that reported in [21] and [10]. The O_2:Ar flow ratio was optimized to result in oxygen rich, low loss films while preventing the sputtering targets from oxidizing. Using the prism coupling method to measure the planar losses around 1550 nm, we determine the background loss and dopant concentration in the Al_2O_3:Er film to be <0.1 dB/cm and 0.9×10^{20} cm^{-3}, respectively.

A series of DFB grating structures with variation in grating strength and cavity length were fabricated. The grating period was 489 nm and a quarter wavelength phase shift in the center created the cavity. The 4-μm-wide waveguide ensures the waveguide is single-mode in the transverse direction and the quarter-wave phase shift design creates a single longitudinal resonant mode in the middle of the optical bandgap. The grating depth variation on each side of the waveguide was $\delta W = 100$, 123, and 145 nm, and the DFB length was varied between 15 and 23 mm. The choice of $N = 0.9 \times 10^{20}$ cm^{-3} for Er ion concentration ensures sufficient gain without excessive pump absorption along the waveguides. Increasing the Er concentration beyond this range would not increase the achievable gain significantly despite higher pump absorption rates, as energy transfer upconversion (ETU) and quenched ion clusters limit the effective excited state lifetime of active ions (τ_{eff}) [22].

The chips were pumped with an 11 watt IPG Photonics RLR 1480 nm Raman fiber laser, using an SM980 (6 μm core diameter) at one edge, and the emitted photons were collected from the other edge. The fiber-to-chip coupling introduced approximately 10 dB loss both for the pump and the emitted signal and no damage was observed, even when more than 1 W of pump power was coupled into the waveguide. DFB devices with stronger width modulation ($\delta W = 123$ and 145 nm) demonstrated single-mode lasing at 1563 nm wavelength while the best slope efficiency of 7 percent was achieved with the strongest cavity design. Figure 2 depicts two sample pump–signal efficiency curves for 145 nm width modulation ($\kappa = 300$) with two different grating lengths. The longer DFB demonstrates 75 mW of on-chip laser power when pumped with 1.1 W, which is, to our knowledge, the greatest power achieved from a chip-based laser in the communication wavelengths. The resolution of the optical spectrum analyzer (OSA) used was 20 pm, and the lack of any beat signal observable on the 50-GHz-bandwidth spectrum analyzer through a high-speed detector confirms the single-mode operation of the laser.

Time-domain analysis of the laser output reveals power fluctuations when the pump rate is not significantly higher than the threshold. Laser output intensity fluctuation is a well-known phenomenon in highly doped rare-earth-based fiber lasers, and is attributed to a combination of self-pulsating due to quenched ion clusters [23] and resonant amplification of pump noise at relaxation frequency [24]. Although it is known that the percentage of quenched Er ions increases with the doping concentration, and is around 10% for $N = 0.9 \times 10^{20}$ cm^{-3}, the excited lifetime of the quenched ions has not been measured [22]. Here, we use an indirect method, based on the relaxation oscillation frequency of the laser, to extract the effective lifetime of all Er atoms and analyze the time-domain performance of the laser, similar to that of [25], done for Yb.

The frequency of relaxation oscillation, which is due to the dynamic interplay of cavity photon density and active ion population inversion, increases with the pump rate intensification, such that [25,26]:

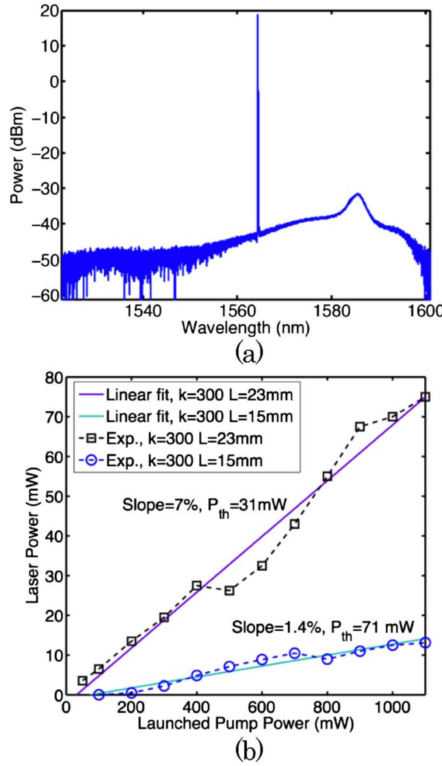

Fig. 2. On-chip DFB laser performance. (a) Single-mode laser emission from the DFB with more than 60 dB suppression of the amplified spontaneous emission (ASE), measured with an OSA with 0.02 nm resolution. The peak around 1588 is due to the Raman-shifted residual pump. (b) Power as a function of launched pump power for two lasers with equal corrugation ($\kappa = 300$), but different grating length ($L = 23$ and 15 mm), lasing at 1563 nm. The cavity with the longer grating shows higher slope efficiency and a lower threshold.

$$\omega_{\mathrm{ro}}^2 = \frac{1}{\tau_{\mathrm{eff}}}\left(\frac{1}{\tau_c} + \frac{c}{n}\sigma_a N\right)\left(\frac{P_p}{P_{\mathrm{th}}} - 1\right), \tag{1}$$

in which ω_{ro} is the angular frequency of relaxation oscillation, τ_{eff} is the effective excitation lifetime of Er ions in $^4\mathrm{I}_{13/2}$ state, τ_c is the cavity lifetime, c is the speed of light, n is the effective refractive index of the waveguide, σ_a is the absorption cross section of Er ions at the laser wavelength, and the $P_{p,\mathrm{th}}$ are the pump and threshold powers. Consequently, the effective lifetime τ_{eff} can be extracted from the y–axis intercept when plotting ω_{ro}^2 as a function of pump rate $r = P_p/P_{\mathrm{th}}$. In Fig. 3, the relaxation oscillation as a function of pump rate for the cavity with the longest lifetime is plotted. Note that, in Eq. (1), the dependence of relaxation oscillation frequency on cavity lifetime is negligible for sufficiently high doping concentration and longer photon lifetimes. This calculation is performed for the cavity with the longest lifetime ($\kappa = 300$, $L = 23$ mm). Coupled mode simulation predicts a quality factor of $Q = 5.4 \times 10^6$, which corresponds to a photon lifetime of 8.3 ns. Considering that the Er absorption cross section at the lasing wavelength (1563 nm) is $\sigma_a = 3.5 \times 10^{21}$ cm^2, and the effective index of the waveguide mode is $n = 1.62$, the effective lifetime of the excited state for the Er ion assembly is calculated to be $\tau_{\mathrm{eff}} = 40$ µs. This is significantly shorter than the

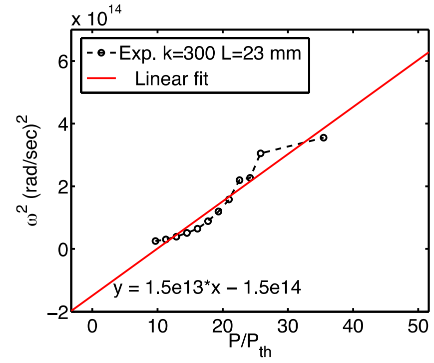

Fig. 3. Relaxation oscillation frequency as a function of pump rate for a DFB laser with an intrinsic lifetime of 8.3 ns ($\kappa = 300$, $L = 23$ mm). The y-axis intercept [$\omega^2 = 1.5 \times 10^{14}$ (rad/s)^2] determines the effective lifetime of the Er ions.

$\tau = 7.55$ ms lifetime reported for the unquenched Er ions in the $\mathrm{Al_2O_3}$ matrix [22]. Considering that the percentage of quenched ions due to undesired impurities, ion pairs and clusters, or host material defects, such as voids,

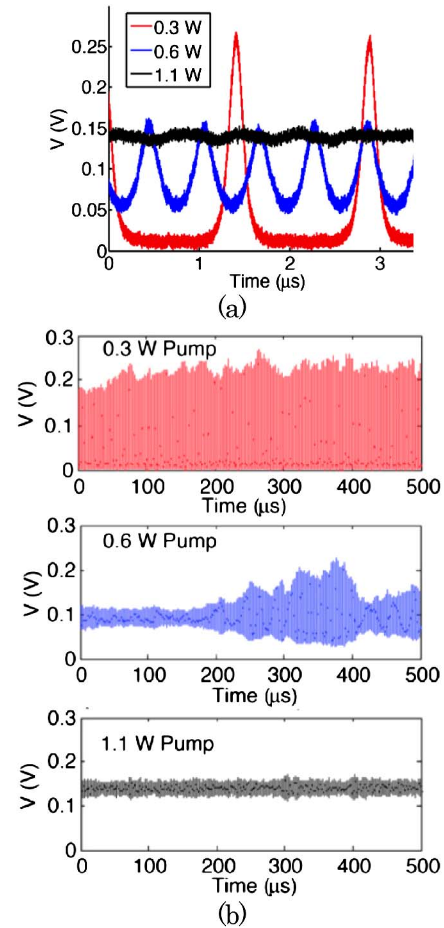

Fig. 4. Effect of pump rate on intensity fluctuations of the laser output power. (a) Self-pulsing behavior is suppressed when the launched pump power is increased from 0.3 W (red) to 1.1 W (black). (b) Laser intensity fluctuation monitored for 0.5 ms. Low pumped case (red) demonstrates sustained self-pulsing behavior while moderately pumped laser (blue) is susceptible to instabilities. The highest pumping setting (black) is stable for a longer period.

depends on the doping concentration, we estimate that as much as ~10% of the ions exhibit extremely short excitation lifetimes [22].

A weighted averaging in the form of [25]

$$\frac{1}{\tau_{\mathrm{eff}}} = \frac{q}{\tau_q} + \frac{1-q}{\tau}, \qquad (2)$$

in which q and τ_q are the quenched ion percentage and lifetime, respectively, reveals that the lifetime of the quenched ions is as short as $\tau_q = 4$ μs. Our rate equation model based on this parameter predicts more stable operation when the laser is excited with a more intense pump. As shown in Fig. 4(a), the measured laser output stability has a strong dependence on pump power. When pumped slightly above threshold ($P = 300$ mW), the laser with $\kappa = 300$ and $L = 15$ mm demonstrated nearly full-scale pulsing with a frequency of 822 kHz. As the pump intensity was increased, the relaxation oscillation frequency increased and pulsing behavior was suppressed. Figure 4(b) also shows the intensity of the laser monitored for 0.5 ms at different pump levels. The low pumping case demonstrates sustained pulsing while the highest pump provides a stable output. When pumped with 600 mW, the laser output fluctuates between a sinusoidal and pulsing behavior (probably due to small variations in pump coupling efficiency from the single-mode fiber to the chip).

In this work we demonstrated high-power, stable, CMOS-compatible Er-doped DFB lasers, with the highest reported single-mode power in SOI-based systems. Pumping at 1480 nm wavelength leads to a 7% slope efficiency for the highest Q cavities and 75 mW of on-chip lasing power at 1563 nm. As the collection of power is done from only one side of the symmetrical device, we expect the possible power extraction to be twice as much as the reported value. Highly doped material is susceptible to intensity fluctuations at lower pump powers but the laser achieves stable operation when pumped with 1.1 W pump power. Longer cavity lifetimes, higher photon density, and elimination of resonant noise from the pump can lead to even more stable laser operation in future.

The authors would like to thank F. Kärtner and E. P. Ippen for invaluable discussions on laser stability experiments. This work was funded by Defense Advanced Research Projects Agency Electronic Photonics Integration (DARPA-EPHI) program, grant no. HR0011-12-2-0007, Samsung Global Research Outreach (GRO) program, and the institute for soldier nanotechnologies.

References

1. S. Keyvaninia, S. Verstuyft, L. Van Landschoot, F. Lelarge, G.-H. Duan, S. Messaoudene, J. M. Fedeli, T. De Vries, B. Smalbrugge, E. J. Geluk, J. Bolk, M. Smit, G. Morthier, D. Van Thourhout, and G. Roelkens, Opt. Lett. **38**, 5434 (2013).
2. S. Srinivasan, A. W. Fang, D. Liang, J. Peters, B. Kaye, and J. E. Bowers, Opt. Express **19**, 9255 (2011).
3. T. Creazzo, E. Marchena, and S. Krasulick, Opt. Express **21**, 28048 (2013).
4. J. D. B. Bradley, R. Stoffer, L. Agazzi, F. Ay, K. Wörhoff, and M. Pollnau, Opt. Lett. **35**, 73 (2010).
5. E. H. Bernhardi, H. A. G. M. Van Wolferen, L. Agazzi, M. R. H. Khan, C. G. H. Roeloffzen, K. Worhoff, M. Pollnau, and R. M. de Ridder, Opt. Lett. **35**, 2394 (2010).
6. E. H. Bernhardi, H. A. G. M. van Wolferen, K. Wörhoff, R. M. de Ridder, and M. Pollnau, Opt. Lett. **36**, 603 (2011).
7. G. Agrawal, Proc. SPIE **1376**, 224 (1991).
8. H. Rong, R. Jones, A. Liu, O. Cohen, D. Hak, A. Fang, and M. Paniccia, Nature **433**, 725 (2005).
9. R. Camacho-Aguilera and Y. Cai, Opt. Express **20**, 11316 (2012).
10. Purnawirman, J. Sun, T. N. Adam, G. Leake, D. Coolbaugh, J. D. B. Bradley, E. Shah Hosseini, and M. R. Watts, Opt. Lett. **38**, 1760 (2013).
11. J. D. B. Bradley, L. Agazzi, D. Geskus, F. Ay, K. Wörhoff, and M. Pollnau, J. Opt. Soc. Am. B **27**, 187 (2010).
12. O. Mahran, M. Helmy, and M. El Hai, J. Appl. Sci. Res. **5**, 1692 (2009).
13. E. H. H. Bernhardi, Q. Lu, H. A. G. M. van Wolferen, K. Wörhoff, R. M. de Ridder, and M. Pollnau, Photon. Nanostruct. Fundam. Appl. **9**, 225 (2011).
14. J. T. Robinson, K. Preston, O. Painter, and M. Lipson, Opt. Express **16**, 16659 (2008).
15. Purnawirman, E. Shah Hosseini, J. D. B. Bradley, J. Sun, G. Leake, T. N. Adam, D. D. Coolbaugh, and M. R. Watts, in *Advanced Photonics 2013* (2013), paper IM2A.4.
16. E. Herth, B. Legrand, L. Buchaillot, N. Rolland, and T. Lasri, Microelectron. Reliab. **50**, 1103 (2010).
17. M.-C. Tien, J. F. Bauters, M. J. R. Heck, D. T. Spencer, D. J. Blumenthal, and J. E. Bowers, Opt. Express **19**, 13551 (2011).
18. J. F. Bauters, M. J. R. Heck, D. John, D. Dai, M. Tien, J. S. Barton, A. Leinse, R. G. Heideman, D. J. Blumenthal, and J. E. Bowers, Opt. Express **19**, 3163 (2011).
19. M. Belt, T. Huffman, M. L. Davenport, W. Li, J. S. Barton, and D. J. Blumenthal, Opt. Lett. **38**, 4825 (2013).
20. N. Sherwood-Droz and M. Lipson, Opt. Express **19**, 17758 (2011).
21. K. Worhoff, J. Bradley, and F. Ay, IEEE J. Quantum Electron. **45**, 454 (2009).
22. L. Agazzi, K. Wörhoff, and M. Pollnau, J. Phys. Chem. C **117**, 6759 (2013).
23. S. Colin, E. Contesse, P. L. Boudec, G. Stephan, and F. Sanchez, Opt. Lett. **21**, 1987 (1996).
24. Y. Barmenkov and A. Kir'yanov, Opt. Express **12**, 3171 (2004).
25. L. Agazzi, E. H. Bernhardi, K. Wörhoff, and M. Pollnau, Appl. Phys. Lett. **100**, 011109 (2012).
26. J. Salcedo, J. Sousa, and V. Kuzmin, Appl. Phys. B **62**, 83 (1996).